Dual-Mechanism Estrogen Receptor Inhibitors Reveal an Ensemble of Binding Modes for Robust Breast Cancer Antagonism

Jian Min[1,2]*, Jerome C. Nwachukwu[3]*, Sathish Srinivasan[3], Erumbi S. Rangarajan[3], Charles C. Nettles[3], Valeria Sanabria Guillen[4], Yvonne Ziegler[4], Shunchao Yan[4,5], Kathryn E. Carlson[1], Yingwei Hou[1], Sung Hoon Kim[1], Scott Novick[6], Bruce D. Pascal[7], Rene Houtman[8], Patrick R. Griffin[3,6], Tina Izard[3], Benita S. Katzenellenbogen[4], John A. Katzenellenbogen[1], Kendall W. Nettles[3]

[1]Department of Chemistry, Cancer Center and University of Illinois at Urbana-Champaign, Urbana IL 61801, USA

[2] State Key Laboratory of Biocatalysis and Enzyme Engineering, Hubei Collaborative Innovation Center for Green Transformation of Bio-Resources, Hubei Key Laboratory of Industrial Biotechnology, School of Life Sciences, Hubei University, Wuhan 430062, P. R. China

[3] Department of Integrative Structural and Computational Biology, The Scripps Research Institute, Jupiter, FL 33458, USA

[4] Department of Molecular and Integrative Physiology, Cancer Center and University of Illinois at Urbana-Champaign, Urbana IL 61801, USA

[5] Department of Clinical Oncology, Shengjing Hospital of China Medical University, Shenyang, Liaoning Province, 110022, P. R. China

[6] Department of Molecular Medicine, The Scripps Research Institute, Jupiter, FL 33458, USA

[7] Omics Informatics LLC, 1050 Bishop St. #517, Honolulu, HI, 96813, USA

[8] Precision Medicine Lab, 5349 AB Oss, The Netherlands

*Contributed equally

Address Correspondence to:

Dr. Kendall W. Nettles
Email: knettles@scripps.edu

Chemistry:
Dr. John A. Katzenellenbogen
Email: jkatzene@illinois.edu

Abstract

Current antiestrogen therapies for estrogen receptor alpha (ERα)-positive breast cancers work only by direct antagonism, using a single side chain that extends outward from the ligand core to disrupt the transcriptional coactivator-binding site via a direct steric interaction that requires precise chemical targeting. Here, we present a new class of antiestrogens with a 7-oxa-bicyclo[2.2.1]heptene sulfonamide core that combines direct antagonism with indirect antagonism, to also modulate the coactivator-binding site indirectly. These dual-mechanism ER inhibitors (DMERIs) fully antagonized the proliferation of breast cancer cells, including tamoxifen-resistant models, irrespective of their side chain structure and substitution site. These inhibitors displayed an ensemble of binding modes and associated receptor conformational sub-states that drive their unique properties, verified with solution structural probes. Dual-mechanism inhibitors of ERα thus represent an approach to therapeutic targeting with robust efficacy, novel binding modes and associated structural perturbations, and greater tolerance for chemical variety in ligand design.

INTRODUCTION

The estrogen receptor (ERα) plays a critical role in breast cancer because it is a major driver of ~70% of these cancers, and in many of these the suppression of ERα function by endocrine therapies is initially quite effective, either by inhibiting the production of estrogens with aromatase inhibitors (AI) or by blocking the activity of the ER with antiestrogens.[1,2] Nevertheless, many ERα-positive breast cancers recur in forms that have become resistant to standard-of-care AIs and/or antiestrogens. Because most still contain ERα, however, it is possible that antiestrogens of novel design might still prove effective in these recurrent cancers.

The pharmacophore for ER antagonism—the set of chemical and molecular features required for this effect—includes structural features of the ligand and conformational features of the ligand-receptor complex. Traditional antiestrogens are generally classified as either selective estrogen receptor modulators (SERMs), which show tissue-selective partial agonist and antagonist activity, or full antagonists, often termed selective estrogen receptor downregulators (SERDs, **Supplementary Fig. 1a-c**).[3-6] Both SERMs and full antagonists have a common ligand structural feature, namely, a ligand core onto which is attached a *single pendant side chain* that requires very precise interaction with the receptor to control the degree of antagonism. These include aminoalkoxy groups exemplified in various SERMs (tamoxifen, raloxifene, bazedoxifene and lasofoxifene) that interact with the receptor with a single H-bond to stabilize the position of the side chain (**Supplementary Fig. 1a**)[7,8]. Full antagonists bind in a rigid fashion like acrylic acids (as in GW5638, **Supplementary Fig. 1b**) or have extended and largely hydrophobic side chains (as in RU 58,668 and fulvestrant) (**Supplementary Fig. 1c**) that bind precisely into the coactivator binding site[9,10].

The ER antagonist action of all of these ligands, whether SERMs or full antagonists, is mediated through this single side chain, which protrudes between helix 3 (h3) and h11 of the ERα ligand binding domain (LBD), where sub-Å differences in the side chain position control the conformational ensemble of the receptor and the degree of antagonism[11,12]. Because these side chains regulate the position of h12 by direct steric contact, traditional antiestrogens are said to work by "*direct antagonism*[13]", where the

ligands are relatively static while shifting the conformational ensemble of the receptor into ligand-specific activity states.

We found that certain ER antagonist ligands operate by a second mechanism called *"indirect antagonism"* [6,13]. This occurs when ligands with bulky cores perturb secondary structural elements within the ligand binding pocket (LBP), typically by shifting the C-terminal end of h11; this movement acts indirectly through the h11-h12 loop to regulate the dynamics of h12 and can be used to fully control the conformational ensemble of the receptor between active and repressive states[14,15]. This indirect antagonism was especially evident in ligands with a 7-oxabicyclo[2.2.1]heptene sulfonamide (OBHS-N) core scaffold, as illustrated by the parental OBHS-N compound **13**, for which we previously published activity data[6] (**Fig. 1a**).

In this work, we show that we can diversify the pharmacophore for ER antagonism by adding structural elements for both direct and indirect antagonism to the OBHS-N ligand core. In their complexes with the ERα LBD, we found that these dual-mechanism inhibitors revealed an unexpected diversity of ligand binding orientations and LBD conformational modes, with some ligands interacting with the receptor in multiple poses. They also provided robust antagonism across different endocrine therapy-resistant breast cancer cell models, with this being enabled through new ligand-receptor interactions. By highlighting the allosteric nature of the LBD that links ligand-induced conformational stabilization to activity state, these dual-mechanism ER inhibitors (DMERIs) greatly expand the ER-antagonist pharmacophore and show that ER antiestrogen design can be productively extended beyond the traditional framework of single side chain, single-mechanism ERα inhibitors.

RESULTS

Dual-mechanism inhibitor design

The orientation of the R_3 substituent on the F-ring with respect to helix 11 is structurally linked to the position of R_1 (for the designation of the E and F rings of OBHS-N, and substituents R_1-R_3, see **Fig. 1a,** with reference to **Supplementary Fig. 1d–f**), and depending on the particular substitutions, the R_1 and R_3 groups could switch positions by a rotation around the S-N bond[6]. Thus, due to ligand dynamics[16], the F-ring could either face outward towards h12 where it is parallel with h11 and the E-ring, or bind inward

with R_1 facing outward. Para-substitutions on the F-ring favor the outward-facing position of R_3, but in both cases a similar shift in h11 is maintained (**Supplementary Fig. 1e**)[6]. Notably, this outward and parallel orientation of both the E and F-rings provides us the opportunity to combine indirect and direct antagonism for dual-mechanism inhibition.

We prepared two sets of OBHS-N compounds substituted with four types of side chains (**Fig. 1a, Supplementary Datasheet 1**), which were placed on either the E-ring or the F-ring. As R_2 and R_3 substituents, we selected aminoalkyl ether groups characteristic of SERMs but some with longer linker links, acrylic acid groups from SERDs like GW5638 or its methyl ester, and a more complex lipophilic side chain found in RU 58,668 (and very similar to fulvestrant). Some benzyl ethers, used as protecting groups in synthetic intermediates, were also investigated. In all cases, R_1 was a trifluoroethyl group. All synthesis involved facile Diels-Alder reactions of various aryl-substituted furans with different vinyl sulfonamide dienophiles, conducted under conditions of thermodynamic control, which favored production of the exo stereoisomers [17-19]. Synthetic routes and experimental details are in **Supplementary Information.**

Dual-mechanism inhibitors, irrespective of their side chain structure and site of substitution, produce full antagonism of breast cancer cell proliferation.

The DMERIs varied in potency, but they inhibited breast cancer cell proliferation to a degree similar to that of fulvestrant (**Fig. 1a–f, Supplementary Dataset 1**). Those with basic side chains showed similar efficacy whether they had the two-carbon linkers found in known SERMS, or three- or four-carbon linkers (**Fig. 1c**). The acrylic acids had lower potencies (**Fig. 1e**), but a methyl ester derivative had higher potency and an efficacy comparable to fulvestrant (**Fig. 1d**). The efficacy of the benzyl-substituted compounds was particularly noteworthy because the benzyl group, which is often used for protection during chemical synthesis, is without precedent as a side chain in antiestrogens (**Fig. 1f and 1h**). Thus, combining indirect and direct antagonism produced a series of compounds all having full antiproliferative efficacy, including those with benzyl side chains. These findings differ markedly from previous work by us[20] and others[5,21-23] on single-mechanisms ER inhibitors, where small changes in the single side chain gave widely

divergent outcomes in terms of efficacy, and they highlight the more restricted chemical and structural requirements needed for good single-mechanism inhibition of ERα activity[20,24,25].

Most of our compounds displayed affinities and potencies in the 10-100 nM range, except for the acrylates, which had μM potencies **(Supplementary Dataset 1**). Because all of the OBHS-N compounds are racemates, we used chiral HPLC to resolve our two most promising compounds **24** and **15**, and we found that one enantiomer of each (**29** from **24**, and **27** from **15**) accounted for essentially all of their affinity and cellular activity (**Fig. 1 g–h**, **Supplementary Dataset 1**). These preferred enantiomers, **29** and **27**, had antiproliferative potencies of 3 and 0.3 nM, respectively (**Fig. 1g–h, Supplementary Datasheet**). We previously published 32 crystal structures of ERα bound to compounds in the OBHS series in which we had consistently found all activity in one enantiomer (1*S,2R,*4*S*)[6,19,26,27], but here we found two of the structures with amine side chain compounds, **16** and **18** (out of 16 structures, of which we are reporting 10 here, **Supplementary Dataset 1**), that displayed the (1*R,*2*R,*4*S*), while the high affinity enantiomer **29** displayed the *1S* configuration.

To verify on-target mechanism of action, we inhibited cell growth with a subset of the compounds at 1 μM and showed pharmacological reversal with increasing doses of estradiol (**Fig. 1i**). We also showed that the compounds effectively antagonized E2 induction of the ER-target gene, GREB1, further supporting their on-target mechanism of action (**Fig. 1j**). Notably, the compounds also showed no effect on proliferation of a triple-negative breast cancer cell line that lacks ERα (**Supplementary Fig. 1g**), again suggesting ER specificity.

Dual-mechanism inhibitors are effective in endocrine-resistance models

To test the suppressive effect of dual-mechanism inhibitors in various endocrine-resistance models, we examined the compounds in MCF-7 cells grown long term in tamoxifen that had developed resistance to Tam (TamR cells) and in MCF-7 cells engineered to express ERα having the activating mutations, Y537S or D538G found in patient tumor samples with endocrine therapy-resistant metastatic disease[28]. These mutations drive constitutive activity by stabilizing the active conformation of ERα, and they reduce the potency of clinically used antiestrogens, such as tamoxifen and fulvestrandt[28]. As expected, the parental compounds (OBHS-Ns with no side chains[6]) were less efficacious in inhibiting proliferation of the Y537S

mutant vs. the wild type ER MCF-7 cells, shown by their activity above the diagonal (**Supplementary Fig. 2a,** Dose curve data for all the compounds is summarized in **Supplementary Dataset 1**). All of the other new compounds showed equivalent inhibition of proliferation against the WT ERα or mutant Y537S ERα cells (**Supplementary Fig. 2a, Supplementary Dataset 1**). Three of the most efficacious compounds, **16**, **27**, and **29**, were selected for more detailed study and comparison with fulvestrant and 4-hydroxytamoxifen (4OHT), the active metabolite of tamoxifen.

Dose-response curves in MCF-7 cells expressing Y537S or D538G ERα (**Fig. 2a–c**) show that fulvestrant lost potency, while 4OHT lost both potency and efficacy. The benzyl-substituted compound **29** also lost potency, but was as efficacious as fulvestrant, as were the other higher potency compounds, **27** and **16** (**Fig. 2a–b**). These inhibitors were also fully efficacious in MCF-7 tamoxifen-resistant cells, TamR (**Fig. 2c**).

Compounds vary in their extent of receptor degradation, and ER degradation does not correlate with anti-proliferative effectiveness

The parental OBHS-N compound **13**, which has only a chlorine as an F-ring substituent, is an effective SERD with ERα degradation efficacy similar to fulvestrant in MCF-7 cells[6]. To our surprise, compounds with larger E- and F-ring substituents showed variable effects on receptor levels, with some having basic side chains, such as **16** and **20**, stabilizing the receptor as does hydroxytamoxifen (**Fig. 2d,** the original gels are shown in **Supplementary Fig. 2b**). However, compounds **24** and **27**, with the benzyl or Roussel side chain, respectively, induced receptor degradation, effects that were reversed by co-treatment with hydroxytamoxifen (4OHT) or proteasome inhibitor MG132, demonstrating on-target mechanism of action through proteasomal degradation (**Supplementary Fig. 2c**).

To understand whether **24** lowers receptor expression through the same mechanism as fulvestrant, we compared effects on mutant ERα missing either the N-terminal transcriptional activation domain (ERα-ΔAB) or with the ligand binding domain fused to a Gal4 DNA binding domain (Gal4-ERαLBD). Fulvestrant was more efficacious than **24** in degrading ERα-ΔAB, while **24** was more efficacious than fulvestrant in degrading Gal4-ERαLBD (**Supplementary Fig. 2d**), illustrating that there are different

structural mechanisms that can modify receptor levels. We also wondered how consistent the degrader phenotype was, so we examined receptor levels across a panel of ERα+ cell lines and found that effects were highly cell-type and ligand-specific (**Supplementary Fig. 2e**). We conclude that effects on receptor levels do not correlate with anti-proliferative effects (**Fig. 1b-h**), although it has been used to probe for ligand-selective differences in receptor conformation in cells, at least in some compound series[29].

Dual-mechanism inhibitors displayed an ensemble of binding modes

We obtained X-ray crystal structures of the ERα LBD in the antagonist conformation in complexes with 10 of the ligands, and with the full antagonist GDC-0810 for comparison. The stereochemistry of the bound higher affinity enantiomer of the E-ring benzyl compound **29** could be unambiguously assigned (as 1*S*,2*R*,4*S*) from the electron density maps (**Supplementary Fig. 3a**). We also obtained the structure of the parental OBHS-N compound, **13**. Compared to the previously published structure bound to the agonist conformer, **13** adopts a new binding mode with the F-ring facing h8 rather than pushing on h11 (**Supplementary Fig. 3b**), allowing h11 to return closer to the agonist conformation, with a shift relative to the estradiol reference structure of only 1.3 Å instead of 2.9 Å (**Supplementary Fig. 3c**). These multiple binding modes suggest that in solution full antagonism only required that some of the receptors are bound by the ligand in the F-ring out conformer to fully distort the agonist conformation.

E-ring amine side chain-substituted ligands showed an ensemble of binding modes, such that only a subset of the E-ring and F-ring positioned amines appeared to support antagonism through known interactions with the receptor. The amine side chains with two carbon linkers found in SERMs are held in place by a tight H-bond with Asp351 in h3. This H-bond positions the head group to control the relative stability of h12 in either the inactive conformer, or destabilized to facilitate corepressor binding, by pushing on Pro535 in the h11-h12 loop, as we previously demonstrated with bazedoxifene (**Supplementary Fig. 3d**)[11]. This shift in Pro535 and the destabilization of h12 accounts for bazedoxifene's efficacy in tamoxifen resistant breast cancer models[30,31]. With **16** and **17**, containing the two and three carbon linkers, the amine group was able to form the H-bond with Asp351, but the head groups shifted Pro535 differently (**Fig. 3d**), despite their similar activity profiles (**Fig. 1c**). With the four-carbon linker, **18**, there was not electron density to support modeling the piperidine amino group, and there was no shift in h11-h12

Pro535 compared to the parental compound **13** (**Fig. 3e**), despite the strong antagonism of this compound in a variety of model systems.

We observed a similar diversity of positioning of the unsubstituted F-rings in support of indirect antagonism, including conformational dynamics within individual ligands. With **16** we observed that 3 of the monomers in the unit cell had the F-ring inward position (**Fig. 3a**), while one monomer had a mixture, with some electron density supporting the F-ring outward conformer (**Fig. 3f**), as well as the accompanying shift in h11 supporting indirect antagonism. In contrast, **17** showed three monomers with the F-ring outward (**Fig. 3b**), and one monomer with a mixture (**Fig. 3g)**. With **18**, the F-ring was disordered in all four monomers, and there was no shift in h11 indicative of indirect antagonism (**Fig. 3e**). Thus, **18**, while being a full antagonist in breast cancer cells, displayed no visible interactions with the known antagonist conformational pharmacophores, while the other amine side chain containing compounds displayed an ensemble of indirect antagonism conformers.

Acrylate-substituted compounds also displayed multiple binding modes. We crystallized **GDC-0810**, and found that its acrylate side chain formed an extensive H-bond with the h11–12 loop, in effect pulling on h12 (**Fig. 3h**), as seen previously with the SERD GW5638[32]. In contrast, the acrylate in **23** was bound internally in all four subunits, displaying a tight hydrogen bond with the base of h3 (**Fig. 3i**, **Supplementary Fig. 3f**), and requiring a substantial shift in the core (**Supplementary Fig. 3e**). This appears to explain its reduced potency compared to the ester, **21**, which formed a weaker H-bond with h3 in 3 of the subunits (**Fig. 3i**, **Supplementary Fig. 3f**). In the fourth subunit of the **21** ER complex, the F-ring faced outward, but here the side chain was also disordered. The positions of V534 and P535 in h11-h12 were not perturbed, demonstrating that we did not visualize ligand-receptor interactions that are typical of antagonist activity.

Atypical side chains access new receptor structural perturbations

F-ring-substituted amine side chains. The aminoalkyl ether substitutions on the F-ring showed new binding epitopes. Compound **19**, with the 2-carbon F-ring aminoalkyl group, positioned the head group exiting between h8 and h11, rather than via the usual exit path between h3 and h11. Consequently, the ether and amino groups H-bonded to His524 rather than Asp351, and in doing so, they pushed h11 by

1.4 Å *towards* h12 (**Fig. 4a**), rather than away from h12, the movement that occurs from the more common exit next to the E-ring. In contrast, **20**, with the F-ring 3-carbon linker, exited towards helix 12 (**Fig. 4b**) and directly contacted the base of h12 (**Fig. 4c**). Here, the head group made VDW contacts with Trp383 in the same location where the Pro535 typically resides in contact with Trp383 (**Fig. 4c-d**). The structure with **20** differs from that of the SERM raloxifene, as the side chain shifted Pro535 across Tryp383, pushing h12 in an orthogonal direction that results in a 2.6 Å difference in the position of h12 (**Fig. 4d**) [33].

Benzyl-substituted systems. We assayed some synthetic intermediates that contained side chain protecting groups because we expected them to serve as inactive, negative controls. The F and E-ring substituted benzyl compounds, **25** and **29**, however, were among the highly efficacious antiproliferative agents (**Fig. 1f, h**). The structure of ERα with **25** resembled the parental compound **13** with the F-ring facing inward, and the side chain was disordered, with no visible indirect or direct antagonism. With the E-ring substituted compound **29**, h12 was disordered in two of the subunits (**Fig.4e**). In the other two subunits, h12 was held in place by crystal packing, enabling visualization of the mechanism through which h12 was disordered: h12 and the h11-h12 loop were shifted towards the benzyl group such that Pro535 was stacked against the benzyl side chain (**Fig. 4e, f**).

Dual-mechanism inhibitors display altered receptor conformation patterns in solution

The position of the F-ring-substituted **20** with respect to h12 suggested it may also have altered interactions with transcriptional coregulators that bind the same surface. Superimposing of the structures of ERα with **20**, and with raloxifene and a corepressor peptide demonstrate that the amino group of **20** is positioned to interact directly with the peptide as well (**Supplementary Fig. 4a**). To test whether compounds having the same groups substituted at E- vs. F-ring positions produced different interaction surfaces in solution, we assayed paired sets of 2- and 3-carbon linked amines for their ERα interaction with 154 peptides, along with a parental compound **30** (**Supplementary Fig. 4b**)[34]. These peptides were selected from known nuclear receptor interacting proteins**.** Estradiol promoted interaction of ERα with a number of peptides, including those from Steroid Receptor Coactivator (SRC) 1–3 coactivators (noted in

the **Fig. 6a**), all of which were strongly dismissed by 4OHT and fulvestrant (**Fig. 5a)**. The E-ring substituted C_2 and C_3 amino alkyls, **16** and **17**, showed patterns similar to those of these antiestrogens, as did the parental compound **30** to a lesser extent (**Fig. 5a**). In contrast, the F-ring substituted C_2 and C_3 alkyl amines, **19** and **20**, had a very different and more muted pattern of peptide interactions (**Fig. 5a**), suggesting that in cells they may display altered interaction with coregulators.

As a further probe of solution structure, we examined the dynamics of secondary structural elements through mass spectrometry analysis of the exchange of amide hydrogens for deuterium (HDX). These included the high affinity enantiomers of the parental compound **31** (derived from 13**,** **Supplementary Fig. 4b**), the F-ring-substituted Roussel side chain compound **27**, and the E-ring substituted benzyl compound **29**. While 4OHT and fulvestrant stabilized the C-terminal half of h11 proximal to the ligands, the dual-mechanism inhibitors **27** and **29** did not, nor did the indirect antagonist **31**, consistent with indirect antagonism directed at h11 (**Fig. 5b, Supplementary Fig. 4c**). All of the compounds stabilized helices 3 and 4 in the AF-2 surface, except for **29**, the compound that destabilized h12 in the crystal structure (**Fig. 5c**, **Supplementary Fig. 4d**). With **27**, the extended hydrophobic side chain may directly contact the AF-2 surface to stabilize its secondary structural elements, as was seen with the fulvestrant analog, ICI 164,384[35] (**Supplementary Fig. 4f**). With the other compounds, the stabilization of the AF-2 surface is likely through h12 binding to the AF-2 surface in the inactive conformer (**Supplementary Fig. 4d**), highlighting the unique ability of **29** to destabilize h12 in solution and in the crystal structure. Lastly, we observed that 4OHT destabilized part of h8 (**Fig. 5d**) and the adjacent h9 across the dimer interface in the Y537S-ERα (**Fig. 5e, Supplementary Fig. 4f**). The reduction in efficacy of 4OHT in the context of the constitutively active Y537S-ERα suggests that it may not be able to efficiently disrupt the constitutively active conformer of h12, and that the side chain may be accommodated internally as we have seen with some of the dual-mechanism inhibitors (e.g. **Fig. 4i**). Flipping the ligand around the phenyl hydroxy group by 180º showed the amino group interacting with the same region of h8 that was destabilized (**Fig. 5f**), further supporting the interaction between ligand and receptor dynamics in regulating receptor activity resistance to tamoxifen in Y537S-ERα.

DISCUSSION

By acting through both direct and indirect antagonism mechanisms, the dual mechanism ER inhibitors (DMERIs) all gave complete suppression of breast cancer cell proliferation. Our structural analyses showed that they displayed an ensemble of ER conformers revealing newly identified structural mechanisms for both direct and indirect antagonism (**Fig. 6a-d**). These differences were reflected in novel patterns of peptide binding (**Fig. 5a**), and by the unusual binding modes of the F-ring aminoalkyl ethers **19** and **20** (**Fig. 4a–d**) and the effects of the E-ring benzyl side chain **29** on melting h12 (**Fig. 4e–f**). Importantly, the ligands themselves also displayed an ensemble of binding orientations and ligand conformational dynamics (**Figs. 3-4**), suggesting that their robust biological effects are associated with a mixture of ligand-receptor sub-states in solution (F**ig. 5b-f**), which likely have low energetic barriers between them as the ligands dissociate and rebind in different orientations (**Fig. 6d**).

Our findings stand in contrast to the traditional view of nuclear receptor allostery, which is based on single, direct-acting mechanisms, and by which the ligand adopts a single pose to control the conformation of the protein (**Supplementary Fig. 6a-c**)[36]. The single-mechanism ligands select or induce lowest energy conformations of the receptor associated with specific activity profiles that can be active, inactive, or mixed (**Supplementary Fig. 6a–d**). The targeting of multiple antagonist sub-states that we can do with DMERIs may provide a therapeutic targeting benefit similar to the effects of targeting multiple growth pathways with combination therapies. This may be especially important in the context of different resistance mechanisms that shift the conformational ensemble to pre-favor the active conformer (**Fig. 6e**), such as with constitutively activating mutants, or can favor the inactive LBD conformer through phosphorylation of ER by several kinase signaling pathways (**Supplementary Fig. 1d**, **6e**) [37-39], where Ser305 in the hinge domain can h-bond to Arg548 just C-terminal to the LBD in the F-domain and stabilize the SERM resistance conformation[39] (**Figure 6c, 6e**). We previously demonstrated that ligand dynamics, with multiple ligand binding conformations, can also drive partial agonism, and utilization of different allosteric signaling pathways through the receptor, and enhanced anti-inflammatory activity of a set of partial agonists [16,40]. Ligand binding ensembles have also been shown to drive allosteric partial agonism of GPCRs and other proteins[41,42].

The ensemble of ligand-receptor complexes we observed with our DMERIs demonstrate that robust antagonism could be achieved with a diversity of ligand designs, including side chains that appeared not to support antagonism in these structural snapshots of the receptor. This suggests that in solution, antagonist ligand poses may need only to be sampled, perhaps only in one monomer of the dimer, although we also visualized ligands fully lacking receptor interactions known to support antagonism (**Fig. 4**). This is reminiscent of the findings that only 10% of the glucocorticoid receptor may need to bind to a response element to engender full agonism and enable the assisted loading of other transcription factors to the same site[43]. With the dual-mechanism inhibitors we report on here, the existence of an ensemble of different antagonist sub-states is likely connected to the wider tolerance for chemical substitutions that has revealed novel aspects of ligand design and allostery. The new dimensions in ligand design opportunities illustrated by these DMERIs may facilitate the development of compounds that are most optimal in targeting metastatic and treatment resistant breast cancers.

Acknowledgments

Supported by the Breast Cancer Research Foundation (BCRF 19-084 and 19-083 to JAK and BSK) and the National Institutes of Health (R01 CA220284 to JAK, BSK, TI, and KWN; and T32 GM070421 Fellowship to VSG), Natural Science Foundation of Hubei Province (2019CFB385 to JM). SS was supported by the Frenchman's Creek Women for Cancer Research, and SY received support from Department of Clinical Oncology, Shengjing Hospital of China Medical University.

Competing Interests

JAK is a founder and stockholder of Radius Health Inc. and a consultant of Celcuity Inc. BSK is a consultant of Celcuity Inc.

Author contributions

Conception/Design of experiments, JM, SHK, PRG, TI, BSK, JAK, KWN. Data acquisition/analysis/interpretation. JM, JCN, ER, SS, CCN, VSG, YZ, SY, KC, YH, SHK, SN, BP, RH, BSK, JAK, KWN. Writing/editing of paper. JM, JCN, BSK, JAK, KWN.

Data availability statement

All of the cell-based raw data is in the Supplementary Dataset 1 and all other raw data is available upon request. X-ray structure PDBs will be deposited upon publication.

REFERENCES

1. Rugo, H.S. et al. Endocrine Therapy for Hormone Receptor–Positive Metastatic Breast Cancer: American Society of Clinical Oncology Guideline. *Journal of Clinical Oncology* **34**, 3069-3103 (2016).

2. Tryfonidis, K., Zardavas, D., Katzenellenbogen, B.S. & Piccart, M. Endocrine treatment in breast cancer: Cure, resistance and beyond. *Cancer Treatment Reviews* **50**, 68-81 (2016).

3. Wardell, S.E. et al. Pharmacokinetic and pharmacodynamic analysis of fulvestrant in preclinical models of breast cancer to assess the importance of its estrogen receptor-alpha degrader activity in antitumor efficacy. *Breast Cancer Res Treat* **179**, 67-77 (2020).

4. Wardell, S.E., Marks, J.R. & McDonnell, D.P. The turnover of estrogen receptor alpha by the selective estrogen receptor degrader (SERD) fulvestrant is a saturable process that is not required for antagonist efficacy. *Biochem Pharmacol* **82**, 122-30 (2011).

5. Guan, J. et al. Therapeutic Ligands Antagonize Estrogen Receptor Function by Impairing Its Mobility. *Cell* **178**, 949-963 e18 (2019).

6. Srinivasan, S. et al. Full antagonism of the estrogen receptor without a prototypical ligand side chain. *Nat Chem Biol* **13**, 111-118 (2017).

7. Jordan, V.C. Antiestrogens and selective estrogen receptor modulators as multifunctional medicines. 1. Receptor interactions. *J Med Chem* **46**, 883-908 (2003).

8. Jordan, V.C. Antiestrogens and selective estrogen receptor modulators as multifunctional medicines. 2. Clinical considerations and new agents. *J Med Chem* **46**, 1081-111 (2003).

9. Wakeling, A.E. & Bowler, J. ICI 182,780, a new antioestrogen with clinical potential. *J Steroid Biochem Mol Biol* **43**, 173-7 (1992).

10. Van de Velde, P. et al. RU 58 668, a new pure antiestrogen inducing a regression of human mammary carcinoma implanted in nude mice. *The Journal of Steroid Biochemistry and Molecular Biology* **48**, 187-196 (1994).

11. Fanning, S.W. et al. The SERM/SERD bazedoxifene disrupts ESR1 helix 12 to overcome acquired hormone resistance in breast cancer cells. *Elife* **7**(2018).

12. Grese, T.A. et al. Molecular determinants of tissue selectivity in estrogen receptor modulators. *Proc Natl Acad Sci U S A* **94**, 14105-10 (1997).

13. Shiau, A.K. et al. Structural characterization of a subtype-selective ligand reveals a novel mode of estrogen receptor antagonism. *Nature Structural Biology* **9**, 359 (2002).

14. Nettles, K.W. et al. Allosteric control of ligand selectivity between estrogen receptors alpha and beta: implications for other nuclear receptors. *Mol Cell* **13**, 317-27 (2004).

15. Nettles, K.W. et al. NFkappaB selectivity of estrogen receptor ligands revealed by comparative crystallographic analyses. *Nat Chem Biol* **4**, 241-7 (2008).

16. Srinivasan, S. et al. Ligand-binding dynamics rewire cellular signaling via estrogen receptor-alpha. *Nat Chem Biol* **9**, 326-32 (2013).

17. Zhou, H.-B., Comninos, J.S., Stossi, F., Katzenellenbogen, B.S. & Katzenellenbogen, J.A. Synthesis and Evaluation of Estrogen Receptor Ligands with Bridged Oxabicyclic Cores Containing a Diarylethylene Motif: Estrogen Antagonists of Unusual Structure. *Journal of Medicinal Chemistry* **48**, 7261-7274 (2005).

18. Zhu, M. et al. Bicyclic core estrogens as full antagonists: synthesis, biological evaluation and structure–activity relationships of estrogen receptor ligands based on bridged oxabicyclic core arylsulfonamides. *Organic & Biomolecular Chemistry* **10**, 8692-8700 (2012).

19. Sharma, N. et al. Exploring the Structural Compliancy versus Specificity of the Estrogen Receptor Using Isomeric Three-Dimensional Ligands. *ACS Chemical Biology* **12**, 494-503 (2017).

20. Min, J. et al. Adamantyl Antiestrogens with Novel Side Chains Reveal a Spectrum of Activities in Suppressing Estrogen Receptor Mediated Activities in Breast Cancer Cells. *J Med Chem* **60**, 6321-6336 (2017).

21. Fanning, S. et al. Specific stereochemistry of OP-1074 disrupts estrogen receptor alpha helix 12 and confers pure antiestrogenic activity. *Nature communications* **9**, 1-12 (2018).

22. Dai, S.Y. et al. Prediction of the tissue-specificity of selective estrogen receptor modulators by using a single biochemical method. *Proceedings of the National Academy of Sciences* **105**, 7171-7176 (2008).

23. Xiong, R. et al. Novel Selective Estrogen Receptor Downregulators (SERDs) Developed against Treatment-Resistant Breast Cancer. *J Med Chem* **60**, 1325-1342 (2017).

24. Miller, C.P. et al. Design, synthesis, and preclinical characterization of novel, highly selective indole estrogens. *Journal of medicinal chemistry* **44**, 1654-1657 (2001).

25. Nwachukwu, J.C. et al. Systems Structural Biology Analysis of Ligand Effects on ERα Predicts Cellular Response to Environmental Estrogens and Anti-hormone Therapies. *Cell Chemical Biology* **24**, 35-45 (2017).

26. Nwachukwu, J.C. et al. Predictive features of ligand‐specific signaling through the estrogen receptor. *Molecular Systems Biology* **12**, 864 (2016).

27. Stender, J.D. et al. Structural and Molecular Mechanisms of Cytokine-Mediated Endocrine Resistance in Human Breast Cancer Cells. *Molecular Cell* **65**, 1122-1135.e5 (2017).

28. Katzenellenbogen, J.A., Mayne, C.G., Katzenellenbogen, B.S., Greene, G.L. & Chandarlapaty, S. Structural underpinnings of oestrogen receptor mutations in endocrine therapy resistance. *Nature Reviews Cancer* **18**, 377-388 (2018).

29. Guan, J. et al. Therapeutic ligands antagonize estrogen receptor function by impairing its mobility. *Cell* **178**, 949-963. e18 (2019).

30. Wardell, S.E., Nelson, E.R., Chao, C.A. & McDonnell, D.P. Bazedoxifene exhibits antiestrogenic activity in animal models of tamoxifen-resistant breast cancer: implications for treatment of advanced disease. *Clin Cancer Res* **19**, 2420-31 (2013).

31. Fanning, S.W. et al. Estrogen receptor alpha somatic mutations Y537S and D538G confer breast cancer endocrine resistance by stabilizing the activating function-2 binding conformation. *Elife* **5**(2016).

32. Wu, Y.L. et al. Structural basis for an unexpected mode of SERM-mediated ER antagonism. *Mol Cell* **18**, 413-24 (2005).

33. Brzozowski, A.M. et al. Molecular basis of agonism and antagonism in the oestrogen receptor. *Nature* **389**, 753-758 (1997).

34. Broekema, M.F. et al. Profiling of 3696 nuclear receptor–coregulator interactions: a resource for biological and clinical discovery. *Endocrinology* **159**, 2397-2407 (2018).

35. Pike, A.C. et al. Structural insights into the mode of action of a pure antiestrogen. *Structure* **9**, 145-53 (2001).

36. Nettles, K.W. & Greene, G.L. Ligand control of coregulator recruitment to nuclear receptors. *Annu Rev Physiol* **67**, 309-33 (2005).

37. Bentin Toaldo, C. et al. Protein Kinase A-induced tamoxifen resistance is mediated by anchoring protein AKAP13. *BMC Cancer* **15**, 588 (2015).

38. Bostner, J., Skoog, L., Fornander, T., Nordenskjold, B. & Stal, O. Estrogen receptor-alpha phosphorylation at serine 305, nuclear p21-activated kinase 1 expression, and response to tamoxifen in postmenopausal breast cancer. *Clin Cancer Res* **16**, 1624-33 (2010).

39. Stender, J.D. et al. Structural and Molecular Mechanisms of Cytokine-Mediated Endocrine Resistance in Human Breast Cancer Cells. *Mol Cell* **65**, 1122-1135 e5 (2017).

40. Bruning, J.B. et al. Coupling of receptor conformation and ligand orientation determine graded activity. *Nat Chem Biol* **6**, 837-43 (2010).

41. Bock, A. et al. Dynamic ligand binding dictates partial agonism at a G protein-coupled receptor. *Nat Chem Biol* **10**, 18-20 (2014).

42. Bock, A. et al. Ligand Binding Ensembles Determine Graded Agonist Efficacies at a G Protein-coupled Receptor. *J Biol Chem* **291**, 16375-89 (2016).

43. Voss, T.C. et al. Dynamic exchange at regulatory elements during chromatin remodeling underlies assisted loading mechanism. *Cell* **146**, 544-54 (2011).

44. Sharma, N. et al. Exploring the Structural Compliancy versus Specificity of the Estrogen Receptor Using Isomeric Three-Dimensional Ligands. *ACS Chem Biol* **12**, 494-503 (2017).

45. Vonrhein, C. et al. Data processing and analysis with the autoPROC toolbox. *Acta Crystallogr D Biol Crystallogr* **67**, 293-302 (2011).

46. Adams, P.D. et al. The Phenix software for automated determination of macromolecular structures. *Methods* **55**, 94-106 (2011).

47. Nwachukwu, J.C. et al. Improved crystallographic structures using extensive combinatorial refinement. *Structure* **21**, 1923-30 (2013).

48. Moriarty, N.W., Grosse-Kunstleve, R.W. & Adams, P.D. electronic Ligand Builder and Optimization Workbench (eLBOW): a tool for ligand coordinate and restraint generation. *Acta Crystallogr D Biol Crystallogr* **65**, 1074-80 (2009).

49. Emsley, P. & Cowtan, K. Coot: model-building tools for molecular graphics. *Acta Crystallogr D Biol Crystallogr* **60**, 2126-32 (2004).

50. Debreczeni, J.E. & Emsley, P. Handling ligands with Coot. *Acta Crystallogr D Biol Crystallogr* **68**, 425-30 (2012).

51. Joosten, R.P., Long, F., Murshudov, G.N. & Perrakis, A. The PDB_REDO server for macromolecular structure model optimization. *IUCrJ* **1**, 213-20 (2014).

52. Aarts, J.M. et al. Robust array-based coregulator binding assay predicting ERalpha-agonist potency and generating binding profiles reflecting ligand structure. *Chem Res Toxicol* **26**, 336-46 (2013).

53. Chalmers, M.J. et al. Probing protein ligand interactions by automated hydrogen/deuterium exchange mass spectrometry. *Anal Chem* **78**, 1005-14 (2006).

54. Zhang, Z. & Smith, D.L. Determination of amide hydrogen exchange by mass spectrometry: a new tool for protein structure elucidation. *Protein science : a publication of the Protein Society* **2**, 522-31 (1993).

55. Pascal, B.D. et al. HDX workbench: software for the analysis of H/D exchange MS data. *J Am Soc Mass Spectrom* **23**, 1512-21 (2012).

56. Keppel, T.R. & Weis, D.D. Mapping residual structure in intrinsically disordered proteins at residue resolution using millisecond hydrogen/deuterium exchange and residue averaging. *J Am Soc Mass Spectrom* **26**, 547-54 (2015).

57. Shiau, A.K. et al. The structural basis of estrogen receptor/coactivator recognition and the antagonism of this interaction by tamoxifen. *Cell* **95**, 927-37 (1998).

58. Webb, P., Nguyen, P. & Kushner, P.J. Differential SERM effects on corepressor binding dictate ERalpha activity in vivo. *J Biol Chem* **278**, 6912-20 (2003).

59. Traboulsi, T., El Ezzy, M., Dumeaux, V., Audemard, E. & Mader, S. Role of SUMOylation in differential ERalpha transcriptional repression by tamoxifen and fulvestrant in breast cancer cells. *Oncogene* **38**, 1019-1037 (2019).

60. Huang, H.J., Norris, J.D. & McDonnell, D.P. Identification of a negative regulatory surface within estrogen receptor alpha provides evidence in support of a role for corepressors in regulating cellular responses to agonists and antagonists. *Mol Endocrinol* **16**, 1778-92 (2002).

METHODS

Cell Culture

MCF7, CAMA-1, MCF7-ERα-WT, MCF7-ERα-Y537S, MCF7-ERα-D538G, T-47D, ZR-75, and MDA-MB231 cells were maintained in Dulbecco's modified eagle medium (DMEM) supplemented with 10% fetal bovine serum (FBS). MCF7-ERα-WT, MCF7-ERα-Y537S, MCF7-ERα-D538G were a gift from Steffi Oesterreich. Ishikawa cells were maintained in DMEM supplemented with 5% FBS. BT-474 cells were maintained in Roswell Park Memorial Institute (RPMI)-1640 medium supplemented with 10% FBS plus 5 µg/ml insulin. MCF7-TamR cells were maintained in phenol red-free RPMI-1640 medium supplemented with 10% charcoal-stripped FBS (Thermo Fisher Scientific, cat no. A3382101) plus 100 nM 4-hydroxytamoxifen. The cells lines above were cultured with 1% penicillin/ streptomycin/ neomycin (PSN) antibiotics, 1% MEM non-essential amino acids, and 1% GlutaMAX (all from Gibco™ by Thermo Fisher Scientific), maintained at 37°C in a 5% CO_2 incubator.

Cell Proliferation Assay

Cells were suspended in steroid-free media supplemented with 10% charcoal-stripped FBS and passed through a 30-micron strainer (Miltenyl Biotec, cat. no. 130-110-915). 25 µl of the cell suspension (i.e. 1,000 or 2,000 cells) was dispensed into each well of 384-well white, flat-bottom microplates (Greiner Bio-One CellStar, cat no. 781080), using a Martix WellMate Microplate Reagent Dispenser (Thermo Fisher Scientific). The next day, test compounds were added to the wells using a Biomek NXP 100-nl pintool (Beckman Coulter). The plates were sealed with Breathe-Easy permeable membranes (Diversified Biotech, Cat no. BEM-1), covered with a stainless steel specimen plate lid (U.S. Patent 6,534,014), and incubated at 37°C and 5% CO2. "Start plates" with replica wells were stored at -80°C to

record the initial number of cells. After 5 days, the start plates were thawed for 15 min at 37°C, and the number of cells/well in all plates were compared. To this end, 25 µl of CellTiter-Glo® assay reagent (Promega, cat no. G7573) was added to each well using the Wellmate reagent dispenser. The plates were shaken gently at room temperature for 5 min on an orbital shaker, and then allowed to sit for 5 min. Luminescence was measured using an Envision plate reader (PerkinElmer). Proliferation data was normalized using the initial number of cells as 0%, and the final number of cells in vehicle (DMSO)-treated wells as 100%.

Quantitative RT-PCR (qPCR)

Total RNA was isolated using the RNeasy kit with on-column DNase I digest (QIAGEN). 4 µg total RNA samples were reverse-transcribed in 40 µl reactions using the High-Capacity RNA-to-cDNA™ Kit (Thermo Fisher Scientific, cat. no. 4387406). cDNA samples were analyzed by real-time PCR in triplicate 10 ul reactions using the 2X TaqMan® gene expression master mix (Applied Biosystems™ by Thermo Fisher Scientific, cat. no. 4369016) with human *GREB1* (Hs00536409_m1) and *GAPDH* (Hs02758991_g1) expression assays. Relative mRNA levels were compared using the ΔΔCt method.

Western Blot

Cells were lysed in ice-cold RIPA buffer (20 mM Tris pH 7.5, 150 mM NaCl, 1% NP40, 0.5% Sodium deoxycholate, 1 mM EDTA and 0.1% SDS). Protein samples were loaded on Any kD™ Mini-PROTEAN® TGX™ Precast Protein Gels (Bio-rad, Hercules, CA) and transferred onto PVDF membranes (Thermo Scientific, Rockford, IL). The membranes were blocked with PBS-T + 5% nonfat dry milk and probed with primary antibodies overnight. The next day, the membranes were washed with with TBS-T, and incubated with HRP-conjugated probes (Santa Cruz Biotechnology) and developed using an ECL detection system (GE Healthcare Bio-Sciences, Pittsburg, PA).

Antibodies and Probes

ERα (F-10) mouse mAb (1:1000, cat. no. sc-8002), ERα (H222) rat mAb (1:1000 dilution, cat. no. sc-53492), β-Actin (C4) mouse mAb (1:10,000 dilution, cat. no., sc-47778), HRP-conjugated mouse IgG kappa binding protein (cat. no., sc-516102), and HRP-conjugated goat anti-rat IgG antibody (cat no. sc-2006), were purchased from Santa Cruz Biotechnology, Inc.

Macromolecular X-ray Crystallography

The ERα-L372S/L536S double-mutant ligand-binding domain (LBD, amino acid residues 298–554) was expressed in BL21 (DE3) E. coli cells, purified by IMAC using a Ni2+ column, dialysis, TEV digest, ion exchange, and size exclusion chromatography to remove the HA tag, as previously described[15]. The purified LBD was co-crystallized with various ligands through sitting drop vapor diffusion method using trial gradients of 20% –25% (w/v) PEG 3350, 200 mM MgCl2, and pH 6.5–8.0, as previously described [40,44]. Data was collected at the Stanford Synchrotron Radiation Lightsource (Beamline: 12-2) and Advanced Photon Source (Beamlines: SER-CAT BM22, ID-22), both at temperature of 100 K and wavelength of 1.0 Å and scaled using AutoPROC [45] with the application of STARANISO (Globalphasing) to accommodate anisotropic diffraction. The structures were solved by molecular replacement of the starting model, 2QXS.pdb, and then rebuilt and refined using the PHENIX software suite version 1.16 [46,47]. Ligand restraints were built on the PHENIX electronic Ligand Builder and Optimisation Workbench [48]. Ligand docking was automated with LigandFit in Phenix and visually inspected using COOT version 0.8.9.2, as previously described [49,50]. New structures were further refined on the PDB-REDO server [51], before final refinement and validation in the PHENIX environment. Structures were analyzed using COOT and imaged using PyMOL (Schrodinger).

MARCoNI coregulator interaction profiling

Microarray assay for real-time nuclear receptor coregulator interaction (MARCoNI) was performed as previously described [52]. In short, a PamChip peptide micro array with 154 unique coregulator-derived NR interaction motifs (#88101, PamGene International) was incubated with his-tagged ERα LBD in the presence of 10 µM compound or solvent only (2% DMSO, apo). Receptor binding to each peptide on the array was detected using fluorescently labeled his-antibody, recorded by CCD and quantified. Per compound, three technical replicates (arrays) were analyzed to calculate the log-fold change (modulation index, MI) of each receptor-peptide interaction versus apo. Significance of this modulation was assessed by Student's t-Test.

Hydrogen-Deuterium Exchange (HDX) detected by mass spectrometry (MS)

Differential HDX-MS experiments were conducted as previously described with a few modifications[53].

Peptide Identification: Peptides were identified using tandem MS (MS/MS) with an Orbitrap mass spectrometer (Q Exactive, ThermoFisher). Product ion spectra were acquired in data-dependent mode with the top five most abundant ions selected for the product ion analysis per scan event. The MS/MS data files were submitted to Mascot (Matrix Science) for peptide identification. Peptides included in the HDX analysis peptide set had a MASCOT score greater than 20 and the MS/MS spectra were verified by manual inspection. The MASCOT search was repeated against a decoy (reverse) sequence and ambiguous identifications were ruled out and not included in the HDX peptide set.

HDX-MS analysis: Protein (10 µM) was incubated with the respective ligands at a 1:10 protein-to-ligand molar ratio for 1 h at room temperature. Next, 5 µl of sample was diluted into 20 µl D_2O buffer (20 mM Tris-HCl, pH 7.4; 150 mM NaCl; 2 mM DTT) and incubated for various time points (0, 10, 60, 300, and 900 s) at 4°C. The deuterium exchange was then slowed by mixing with 25 µl of cold (4°C) 3 M urea and 1% trifluoroacetic acid. Quenched samples were immediately injected into the HDX platform. Upon injection, samples were passed through an immobilized pepsin column (2mm × 2cm) at 200 µl min^{-1} and the digested peptides were captured on a 2mm × 1cm C_8 trap column (Agilent) and desalted. Peptides were separated across a 2.1mm × 5cm C_{18} column (1.9 µl Hypersil Gold, ThermoFisher) with a linear

gradient of 4% - 40% CH_3CN and 0.3% formic acid, over 5 min. Sample handling, protein digestion and peptide separation were conducted at 4°C. Mass spectrometric data were acquired using an Orbitrap mass spectrometer (Exactive, ThermoFisher). HDX analyses were performed in triplicate, with single preparations of each protein ligand complex. The intensity weighted mean m/z centroid value of each peptide envelope was calculated and subsequently converted into a percentage of deuterium incorporation. This is accomplished determining the observed averages of the undeuterated and fully deuterated spectra and using the conventional formula described elsewhere[54]. Statistical significance for the differential HDX data is determined by an unpaired t-test for each time point, a procedure that is integrated into the HDX Workbench software[55]. Corrections for back-exchange were made on the basis of an estimated 70% deuterium recovery, and accounting for the known 80% deuterium content of the deuterium exchange buffer.

Data Rendering: The HDX data from all overlapping peptides were consolidated to individual amino acid values using a residue averaging approach. Briefly, for each residue, the deuterium incorporation values and peptide lengths from all overlapping peptides were assembled. A weighting function was applied in which shorter peptides were weighted more heavily and longer peptides were weighted less. Each of the weighted deuterium incorporation values were then averaged to produce a single value for each amino acid. The initial two residues of each peptide, as well as prolines, were omitted from the calculations. This approach is similar to that previously described[56]. HDX analyses were performed in triplicate, with single preparations of each purified protein/complex. Statistical significance for the differential HDX data is determined by t test for each time point, and is integrated into the HDX Workbench software [55].

FIGURES

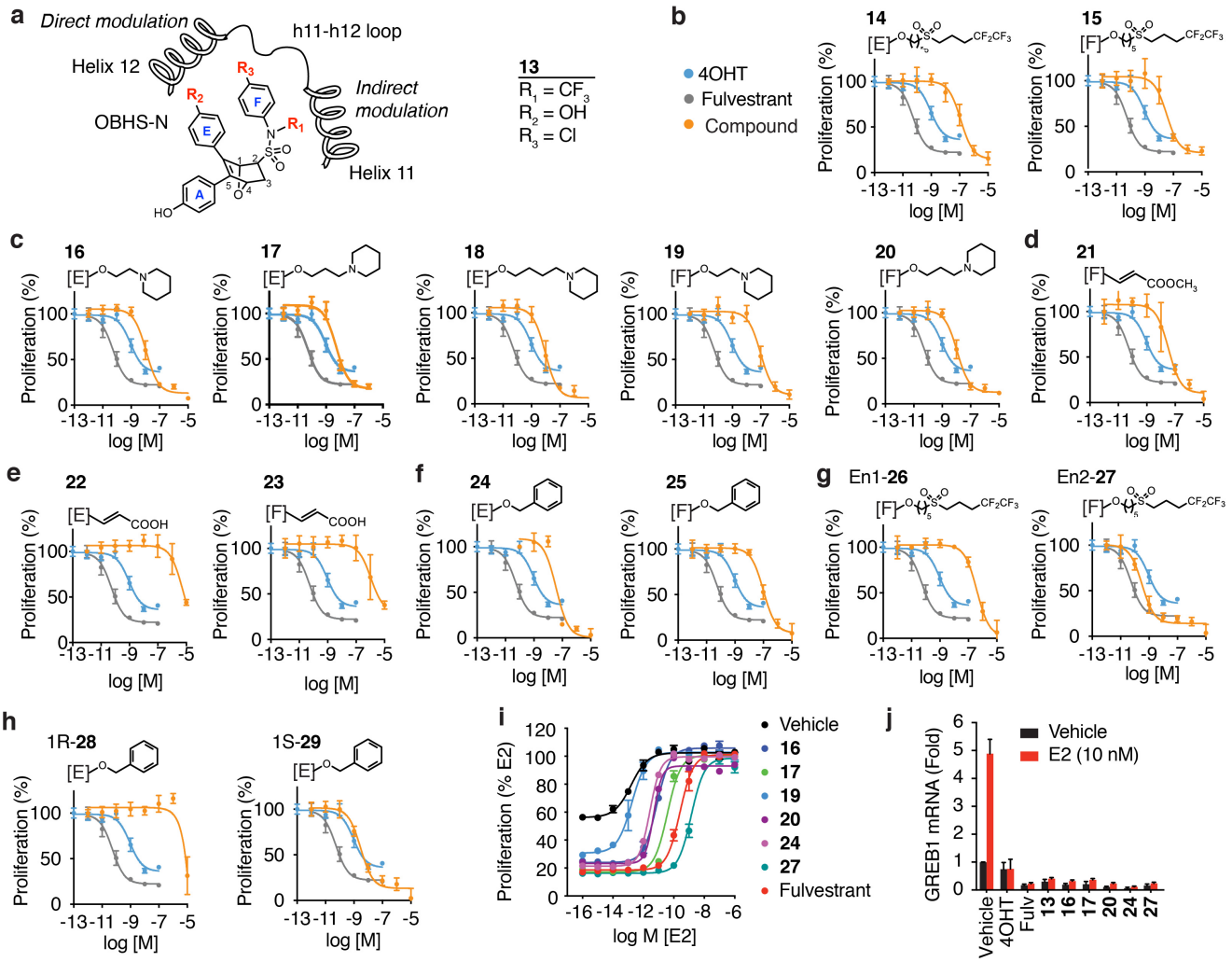

Figure 1. Dual-mechanism ERα inhibitors fully suppress breast cancer cell proliferation and E2-stimulated gene expression regardless of ligand side chain

a) Chemical structure of the OBHS-N scaffold and the orientation of substituents R_1, R_2, and R_3 with respect to h11 and h12 in the ERα LBD. (**b-h**) MCF-7 cells were treated for 5 days with 4OHT, fulvestrant, or the indicated compounds. N= 6 x 8 doses.
b) Roussel side chains attached to the E/F-ring.
c) Basic side chains.
d) Ester side chains.
e) Acrylic acid side chains.
f) Benzyl ether side chains.
g) Separate enantiomers of **15**.
h) Separate enantiomers of **24**.
i) Reversal of the antiproliferative effect by increasing concentrations of E2. MCF-7 cells were treated with the indicated compounds at 1 μM and cotreated with increasing doses of E2. Proliferation was measured after 5 days. N = 3.
j) Ligand-dependent suppression of E2-stimulated *GREB1* mRNA expression. MCF-7 cells were treated with 1 μM of the indicated compounds ± 10 nM E2 for 24 h and analyzed by qPCR. N = 3.
Data are mean ± s.e.m. See also **Supplementary Figure 1**, **Supplementary Dataset 1**

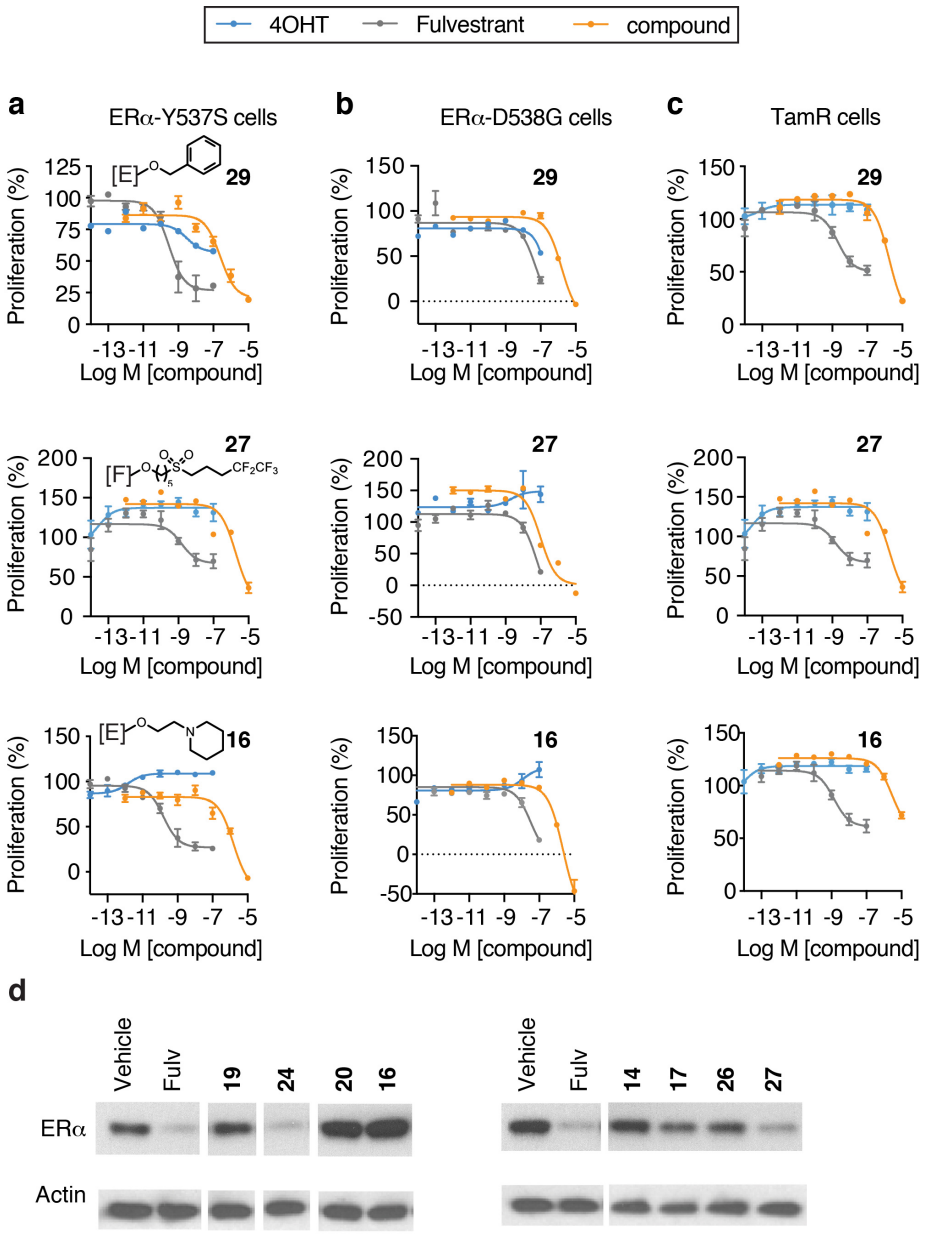

Figure 2. Dual-mechanism inhibitors are effective in suppressing proliferation of mutant ERα expressing cells and tamoxifen-resistant cells.

a-b) Dose-response curves for compounds **29**, **27**, and **16** in MCF-7 cells engineered to express **a**) ERα-Y537S or **b**) ERα-D538G. N = 3 x 8 doses.

c) Dose-response curves for indicated compounds in tamoxifen-resistant MCF-7 cells (TamR) treated as in panel **b**. N = 3 x 8 doses.

d) MCF-7 cells were treated with the indicated compounds for 24 hr. Whole cell lysates were analyzed by Western blot for ERα and β-actin.

Data are mean ± s.e.m. See also **Supplementary Figure 2**

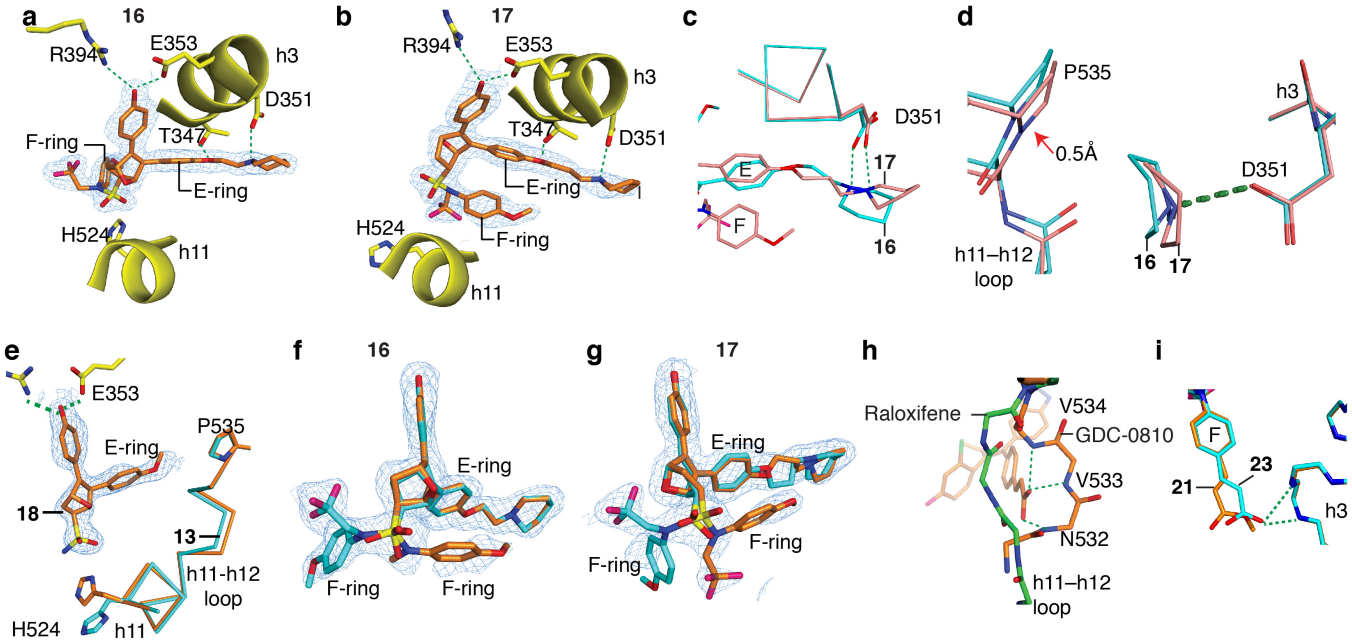

Figure 3. X-ray crystal structures of ERα LBD DMERI complexes reveal dynamic ligand binding and sampling of antagonist binding modes.

a) Structure of **16**-bound LBD showed an internal position of the F-ring in 3 of 4 monomers with $2F_o$-F_c electron density maps contoured at 1.0 σ.
b) Structure of **17**-bound LBD showed an internal position of the F-ring in 3 of 4 monomers with $2F_o$-F_c electron density maps contoured at 1.0 σ.
c) Comparison of **16**- and **17**-bound LBDs shows differential positioning of the amino head groups to achieve an H-bond with h3 Asp351.
d) Comparison of **16**- and **17**-bound LBDs shows how position of amino head group impacts position of the h11-h12 loop.
e) In the **18**-bound LBD, the amino side chain and F-rings are disordered, and do not impact the position of the h11-h12 loop, compared to the structure bound to **13** (blue).
f-g) $2F_o$-F_c electron density map contoured at 1.0 σ shows a mixture of F-ring locations for **16** or **17** in an LBD subunit.
h) The **GDC-0810**-bound LBD shows H-bonding and remodeling of the h11-h12 loop, unlike the raloxifene-bound LBD (2QXS.pdb).
i) The **21**- and **23**-bound LBDs show the F-rings binding internally and H-bonding with the h3 N-terminus. See also **Supplementary Figure 3**

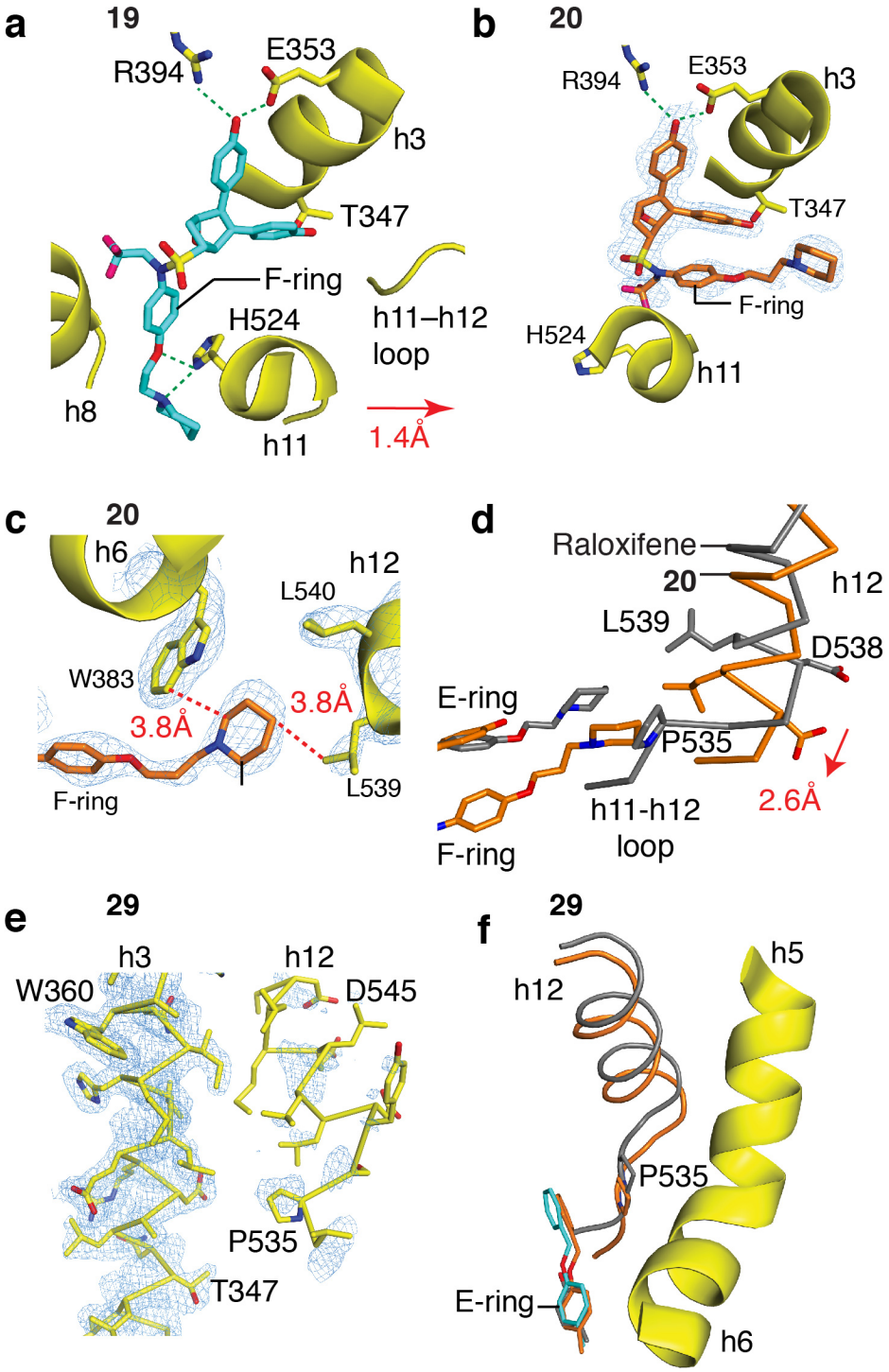

Figure 4. Identification of novel antagonist ligand binding epitopes

a) The side chain of **19** exits the ligand-binding pocket between h8 and h11 and H-bonds to His524, shifting h11 towards h12.

b) $2F_o$-F_c electron density map contoured at 1.0 σ. shows the **20** F-ring facing outward.

c) The pyrrolidine ring of **20** binds between Trp383 in h6 and Leu539 in h12

d) Pyrrolidine ring of **20** binds in place of Pro535, inducing a 2.6 Å shift in h12 compared to raloxifene

e) $2F_o$-F_c electron density map (contoured at 1.0 σ.of an LBD subunit where **29** caused h12 to be largely disordered.

f) Comparison of **29** (orange and blue) with **13** (gray), where h12 is ordered but shifted towards the benzyl side chain. The ligand in the subunit with a disordered h12 is colored blue.

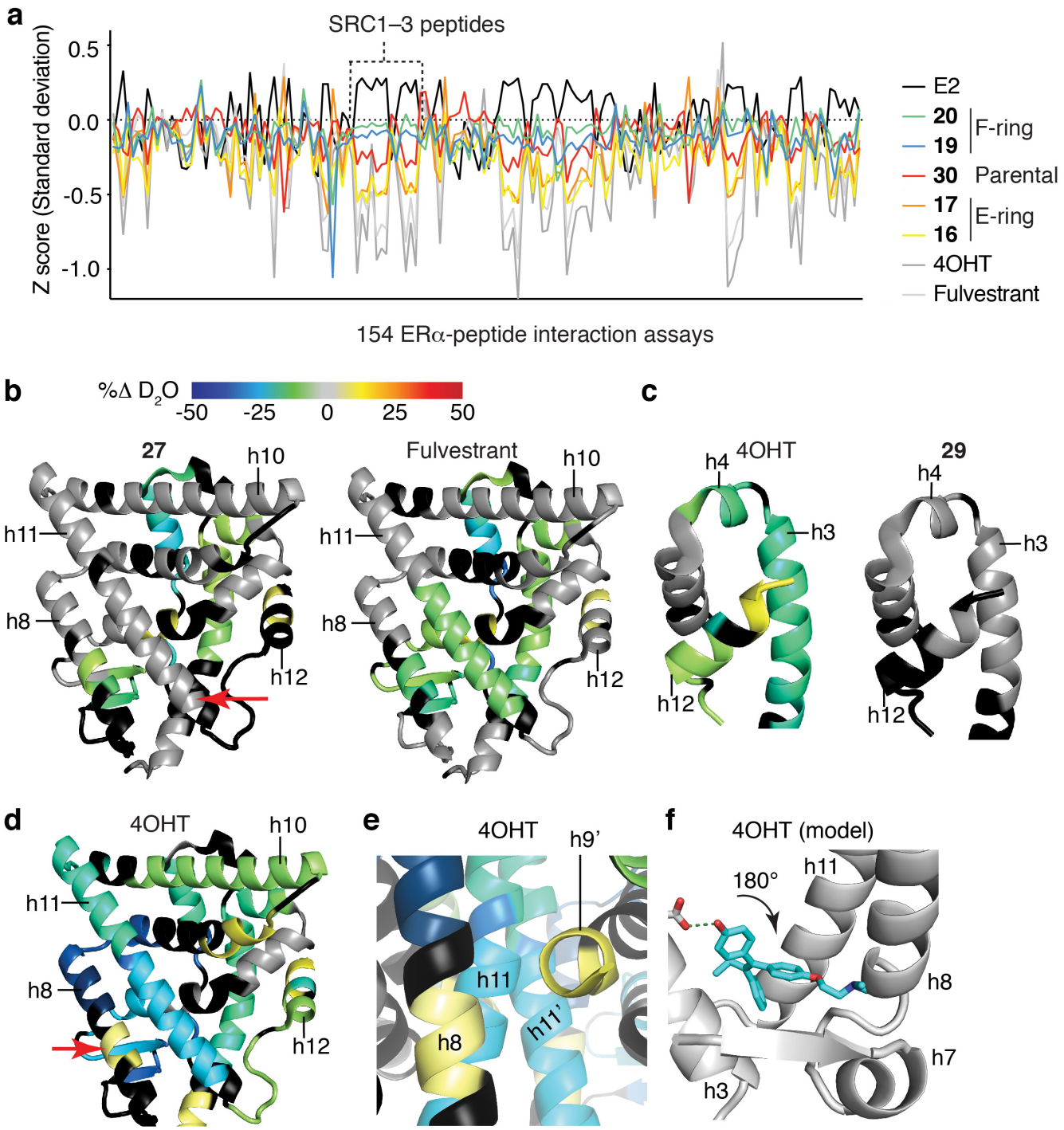

Figure 5. Effects of dual mechanism inhibitors on solution structure of ERα

a) MARCoNI assay for interaction of full-length ERα with 154 peptides derived from nuclear receptor-interacting proteins, including SRC1-3 following treatment with the indicated ligands.

b-d) Hydrogen deuterium exchange mass spectrometry (HDX) analysis of the ERα-Y537S LBD shows comparison of amide exchange rates for the indicated ligand compared to apo receptor.

d-e) In the HDX-MS experiment, 4OHT binding destabilized part of ERα-Y537S **d**) h8 (red arrow), and **e**) the adjacent C-terminal end of h9 across the dimer interface.

f) Model of 4OHT-bound ERα with the side chain flipped to an internal position around the 4OH-phenyl suggesting that the dimethylamine side chain contacts h8. See also **Supplementary Figure 5**

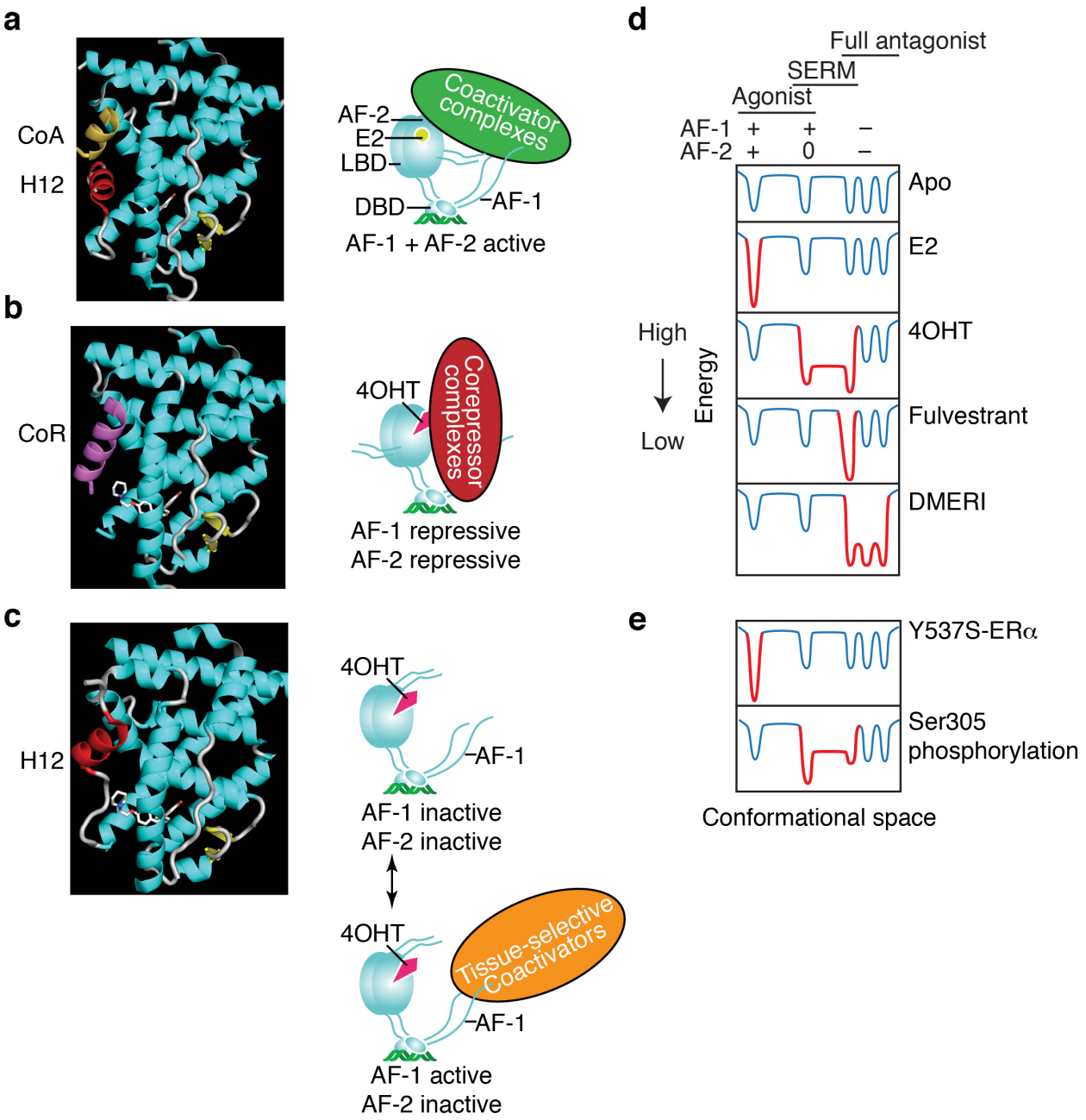

Figure 6. Ligand-dependent control of ERα-LBD conformation, and of ERα coregulator recruitment and selection of activity states.

a-c) The ligand binding domain (LBD) of ERα exhibits three main conformers: an active conformer where agonists stabilize helix 12 (h12) to form one side of a binding site for transcriptional coregulators [57], called Activation Function-2 (AF-2); a repressive conformer where h12 is destabilized enabling recruitment of transcriptional corepressors that mediate chromatin condensation [5,35,58,59]; and an inactive conformer where h12 blocks both coactivators and corepressors[39,57].

a) The active LBD conformation. *Left*, ribbon diagram of the ERα-LBD bound to estradiol. Helix 12 (h12, colored red) forms one side of the coactivator binding site, shown here binding to a peptide from Steroid Receptor Coactivator-2 (CoA colored yellow) 3UUD.pdb. *Right*, Schematic of ERα bound to estradiol (E2), DNA, and a coactivator complex. With full agonists, the coactivator recruitment to the LBD surface, AF-2 (Activation Function-2) nucleates binding of multi-protein coactivator complexes to other domains

including AF-1 (Activation Function-1). DBD, DNA binding domain. Steroid Receptor Coactivators (SRCs) 1–3 bind to both AF-1 and AF-2 through separate interactions.

b) The transcriptionally repressive LBD conformation. *Left*, ribbon diagram of the ERαLBD bound to a corepressor peptide, colored violet. When h12 is disordered by an antagonist, the LBD can bind an extended peptide motif found in transcriptional corepressors[60]. 2JFA.pdb. *Right*, Cartoon of ERα bound to 4-hydroxytamoxifen (4OHT) and a corepressor complex, repressing both AF-1 and AF-2 activity and mediating mediate chromatin compaction and inhibition of proliferative gene expression.

c) The inactive LBD conformer. *Left*, Ribbon diagram of the ERα-LBD bound to an antagonist. Antagonists can flip h12 (colored red) into the coactivator/corepressor binding site, rendering the LBD inactive by blocking both coactivator and corepressor binding to AF-2. 2QXS.pdb. *Right*, when h12 blocks both coactivators and corepressors from binding the LBD, the activity of AF-1 is cell-type specific, as certain tissues such as bone or endometrium have high levels of certain coactivators that bind AF-1.

d) Energy diagram illustrating how ER ligands differ in stabilizing specific low energy receptor conformations associated with transcriptional activity (+), inactivity (0), or repression (–) that are being driven by the activity state of AF-2 or AF-1. The dips in the curves represent different LBD conformations associated with the three AF-1/AF-2 activity states shown at the top, *leftmost* being the active state ***(a)***, the *rightmost* representing sub-states of the repressive state ***(b)***, and the *middle* the inactive state ***(c)***. When a state is stabilized by a particular type of ligand, the curves become deeper, with gray changed to red; the barrier heights between states indicate the ease of dynamic interchange among the states or sub-states. The dual-mechanism ER inhibitors (DMERI) showed multiple mechanisms of antagonism (represented by the multiple favored repressor sub-states with reduced exchange barriers), including direct and indirect, as well as novel interactions with the receptor including melting h12, directly contacting h12, and binding between h11 and h8 (shown in **Fig. 5**).

e) ERα-dependent tamoxifen resistance. Constitutively activating mutations such as ERα-Y537S stabilize the active conformer of AF-2[15]. Phosphorylation of Ser305 in the hinge domain enables an H-bond that stabilizes h12 in the inactive conformer, blocking corepressors and enabling AF-1 activity [39].